HOSTED BY

ELSEVIER

Available online at www.sciencedirect.com

ScienceDirect

Journal of Magnesium and Alloys 4 (2016) 319–325
www.elsevier.com/journals/journal-of-magnesium-and-alloys/2213-9567

Full Length Article

Effect of Gd addition on microstructure and corrosion behaviors of Mg–Zn–Y alloy

Jinyang Zhang, Min Xu, Xinying Teng *, Min Zuo

School of Materials Science and Engineering, University of Jinan, No. 336 West Road of Nan Xinzhuang, Jinan 250022, China

Received 11 June 2016; revised 24 September 2016; accepted 29 September 2016

Available online 7 October 2016

Abstract

The $Mg_{97-x}Zn_1Y_2Gd_x$ alloys were prepared by as-casting method. Corrosion performance of alloys was evaluated by using potentiodynamic polarization, hydrogen evolution rate and mass loss measurements in 3% sodium chloride solution at room temperature. The results shown that the atomic rate of the long period stacking ordered (LPSO) with the composition of $Mg_{12}Zn_1Y_1$. The microstructure of LPSO phases was lamellar structure. When the atomic fraction of Zn is 1% and the atomic ratio of Zn/RE (Y, Gd) is 2:5, the volume fraction of LPSO phase can reach the extreme value. The corrosion resistance of Mg–Zn–Y alloy improves with the increase of the volume fraction of LSPO phase. The $Mg_{96.5}Zn_1Y_2Gd_{0.5}$ (MG0.5) alloy had better corrosion resistance than those of other alloys. It meant that 0.5 at. % gadolinium (Gd) was a suitable addition to $Mg_{97}Zn_2Y$ alloy about corrosion resistance.

Keywords: Magnesium alloy; Gadolinium; Microstructure; Corrosion

1. Introduction

Magnesium (Mg) alloy has been widely used in industrial, spaceflight, electronics and so on due to their high strength weight ratio and low density [1–4]. To stimulate more applications of green materials, some outstanding properties such as easy recyclability and good biocompatibility, which alleviate the shortage of resources and take a dawn to some patients respectively, also has been a concern [5–7]. To acquire admirable properties, a number of investigators have been absorbed in exploring the strengthening phases in Mg alloy [8–12].

In recent years, Mg alloy containing long-period stacking ordered structures (LPSO) has absorbed more attention for its notable microstructure and excellent mechanical properties. Various rare elements (such as Gd, Nb, La, Ce, Eu and Yb) were added into Mg–Zn alloys to form LPSO structures by different processing technology [13–15]. The atomic ratio of the Zn/RE was an important factor for the formation of LPSO structures. The LPSO structure had included various types, such as 10H, 14H, 18R, and 24R (number–number of stacking layers, H-hexahedral structure, and R-rhombus structure). The excellent tensile strength has attained to 610 MPa and the elongation had 5% at room temperature in $Mg_{97}Zn_1Y_2$ RS P/M alloys [16]. The LPSO structure phases were also observed in $Mg_{97}Y_2Zn$ alloy by conventional copper mold casting method [17]. Although many studies have investigated the influence of LPSO phase on the mechanical properties, rare literatures about corrosion resistance can be provided reference. The Gd element has just a higher solid solubility than that of Y and can also produce LPSO structure phase. Therefore, a further investigation about Mg–Zn–Y alloy with Gd additions was investigated.

The study aimed at microstructure and corrosion behaviors of the Mg–Zn–Y–Gd alloy by an as-casting method. It was necessary to optimize microstructure by studying microstructure evolution of LPSO phase and α-Mg phase in Mg–Zn–Y–Gd alloys. The different microstructure had a diverse effect on corrosion resistance. Therefore, an investigation on the microstructure and corrosion behaviors of LPSO phase and α-Mg phase in the Mg–Zn–Y–Gd alloys had been carried out.

2. Experimental procedures

The investigated alloys were prepared from commercial Mg ingot (99.90 wt. %), commercial Zn ingot (99.90 wt. %),

* Corresponding author. School of Materials Science and Engineering, University of Jinan, No. 336 West Road of Nan Xinzhuang, Jinan 250022, China. Fax: +86 531 82765314.

E-mail address: mse_tengxy@ujn.edu.cn (X. Teng).

http://dx.doi.org/10.1016/j.jma.2016.09.003

commercial Mg–Y (29.00 wt. %) master alloy and commercial Mg–Gd (29.96 wt. %) master alloy in an electric resistant furnace under protective atmosphere. At first, Mg ingots were melted in a graphite-clay crucible at 750 °C. Second, the Mg–Y and Mg–Gd master alloys were put into the melt. Then Zn was added to the melt, and held for 10–15 min at 750 °C. Finally the melt was poured into a swage which was pre-heated to 100 °C and cooled at room temperature.

The morphology and structure of the samples were ascertained using an X-ray diffraction (XRD, D8 Advance, Germany) with Cu Kα radiation (λ = 0.154 nm) for phase analyses, a scanning electron microscope (SEM, FEI QUANTA FEG 250) coupled with an energy dispersive X-Ray spectroscopy (EDS) for elemental analyses and differential scanning calorimetry (DSC) for phases formation of alloy. The LPSO structure crystal structure was investigated by the transmission electron microscopy (TEM, JEOL, 2100F, Japan). The sample for TEM was dimpled down to about 20 um, which was achieved by ion milling after mechanically polished. The samples of back scattered diffraction SEM had been eroded with 4 wt. % HF before being tested. Corrosion behaviors of all samples were tested using anodic polarization curves and measured by electrochemical potentiodynamic polarization tests with a potential sweep rate of 1.0 mV/s. All the electrochemical measurements were performed on EC500 electrochemical workstation with a modified sample as working electrode, a saturated calomel electrode (SCE) as reference electrode and a Pt sheet as counter electrode. Prior to all measurements, the surface (for exposing to the solution) of each sample (above 15–20 mm^2) was polished with 2000-grit SiC papers, following by ethanol and deionized water ultrasonic cleaning. The undesired sides of the samples were coated with the epoxy resin. The electrolyte was used by 3% sodium chloride solution at atmosphere. Potentiodynamic polarization curves were scanned after the corrosion samples immersed in the electrolyte for ~1400 s until the open-circuit potential almost reached a steady state. The mass loss samples were immersed into a glass container with 1500 ml 3% sodium chloride solution. The hydrogen evolution was collected by Song G's method [18]. The tested time was controlled by 12 hours every time. Minimum three specimens were carried out for EDS and corrosion rates and average value was reported.

3. Results

3.1. Microstructures of the MG, MG0.5, MG1 and MG2 alloys

The nominal compositions and named are listed in Table 1. The XRD patterns of alloys are shown in Fig. 1. It can be seen that α-Mg phase and LPSO phase ($Mg_{12}Y_1Zn_1$) exist in the $Mg_{97-x}Zn_2YGd_x$ alloy, which are in correspondence to the JCPDF No. 65–4747 and No. 65–3456, respectively. The recent studies presented that LPSO phases were an ordered and hexagonal structure of ACBCBCBACACACBABABA (a = 0.321 nm, c = 4.86 nm) and were formed in alloy solidification stage [19]. The Mg, Y and Zn have an ordered sequence in the LPSO phase. Kawamura and Yamasaki found that LPSO phases formed in $Mg_{97}Zn_1Gd_2$ and $Mg_{97}Zn_1Y_2$ by the as-casting method [17].

Table 1
Nominal atomic compositions of the studied alloys (at.%).

Alloy	Mg	Zn	Y	Gd	Named
$Mg_{97}Zn_2Y_1$	Bal.	1	2	0	MG
$Mg_{96.5}Zn_2Y_1Gd_{0.5}$	Bal.	1	2	0.5	MG0.5
$Mg_{96}Zn_2Y_1Gd_1$	Bal.	1	2	1	MG1
$Mg_{95}Zn_2Y_1Gd_2$	Bal.	1	2	2	MG2

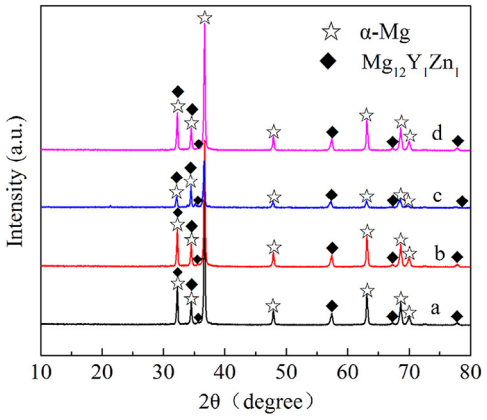

Fig. 1. The XRD patterns of $Mg_{97-x}Y_2ZnGd_x$ alloys: (a) $Mg_{97}Y_2Zn_1$; (b) $Mg_{96.5}Y_2Zn_1Gd_{0.5}$; (c) $Mg_{96}Y_2Zn_1Gd_1$; (d) $Mg_{95}Y_2Zn_1Gd_2$.

The microstructures of alloys are presented in Fig. 2. As Fig. 2 shows, the bright white needle phase is LPSO phase. The black phase is α-Mg matrix phase. The LPSO phase occurs on grain boundaries and exists in the eutectic structure. The grain size of α-Mg matrix phase becomes smaller with the Gd addition. The atomic fraction of Mg–Zn–Y-Gd alloy, with n(Zn)/n(Y + Gd) = 2:5, the volume fraction of LPSO phase can reach the extreme value. The MG0.5 alloy is the well-distributed and net-like LPSO phase on the grain boundary. The reason can be that the atomic ratio of MG0.5 alloy can balance the requirement of the dissolution of Zn and the formation of LPSO phase. When the Gd addition overflows the 0.5 at.%, the increased Gd decreases the formation of LPSO phase. Because some Gd integrated in α-Mg matrix may be increased. The results reveal that RE(Y, Gd) with 2.5at. % addition can be the suitable addition to form the large volume fraction of LPSO phase.

The selected electron diffraction and high magnification dark field image of LPSO of MG1 alloy are presented in Fig. 3. The needle LPSO phase is the 18R structure.

Fig. 4 shows the SEM and EDS results of LPSO phase. As Fig. 4 (1, 2) EDS shows, Y and Zn have a specific atomic ratio that was approached to 1/1, the ratio is considered to the $Mg_{12}Y_1Zn_1$ by Lee and Kim studied [20]. The LPSO phase has been formed in Mg–Zn–RE alloys with hexagonal closed packed (HCP) structure. The formation requirements of LPSO phase was the solid solubility was above 3.75at.% and the atomic size was as larger than that of Mg by 8.4% to 11.9% [19]. The Y and Gd met all the formation requirements, and some studies also confirmed [19]. LPSO phases is formed in

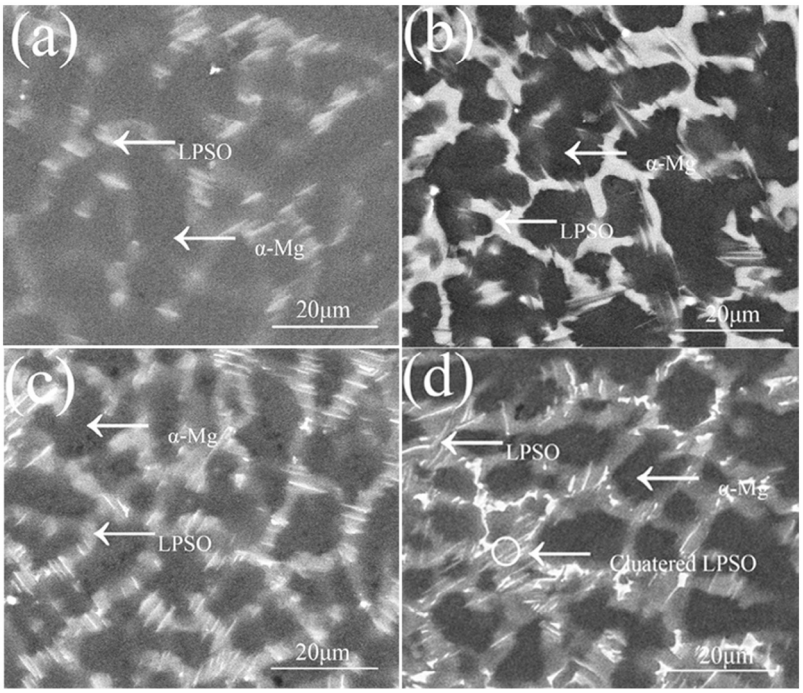

Fig. 2. SEM of $Mg_{97-x}Zn_1Y_2Gd_x$ alloys: (a) $Mg_{97}Y_2Zn_1$; (b) $Mg_{96.5}Y_2Zn_1Gd_{0.5}$; (c) $Mg_{96}Y_2Zn_1Gd_1$; (d) $Mg_{95}Y_2Zn_1Gd_2$.

$Mg_{97}Zn_1RE_2$ alloys with RE = Y, Gd. The LPSO phase is presented light white portion, shown in Fig. 4. The composition of LPSO phase of MG0.5 alloy is $Mg_{92.00}Zn_{3.65}Y_{3.34}Gd_{1.00}$ (at. %). It can be illustrated that Gd and Y existed in the LPSO phase at the same time.

Fig. 5 shows the results of DSC during the cooling process. Two exothermic peaks have been found during the cooling process. It means that the formation of two phases is seen in studied alloys. It is similar to XRD investigated results that two phases are shown in experiment alloys with decreasing temperature, α-Mg formed first in $Mg_{95}Y_2Zn_1Gd_2$ (MG2) alloy with equation L→ L + α-Mg at around 608 °C; then LPSO was produced by liquid and α-Mg with a formula L + α-Mg → LPSO at about 510 °C. The freezing points of α-Mg and LPSO are on the decreasing. One reason may be that solidification of α-Mg needed more energy due to the increased LPSO phase during cooling process. The other reason is that super-cooling should satisfy the growth of atomic cluster of LPSO during precipitation process.

3.2. Corrosion behavior

The polarization curves of $Mg_{97-x}Y_2ZnGd_x$ alloys were measured using the electrochemical workstation (EC500). The relationship between the corrosion current density and potential is accord with Tafel's law in weak polarization region [18,21,22]. It was well known that pretty corrosion resistance means high self-corrosion potential (E_{corr}) and low self-corrosion current density (i_{corr}) [23]. The i_{corr} indicated corrosion rate, and the corrosion potential is related to the component, phase constituent and distribution of phases. It is generally known that the negative difference effect is the common condition in Mg alloy. The corrosion rates of Mg–Zn–Y–Gd alloys were calculated

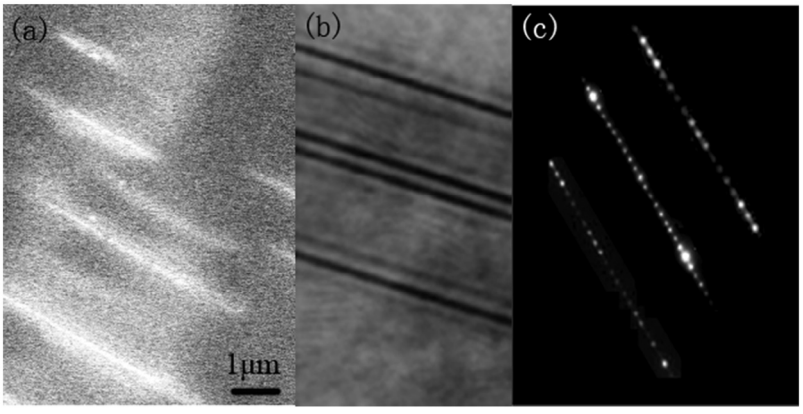

Fig. 3. (a) SEM image of LPSO, (b) high magnification bright field image of LPSO phases, and (c) corresponding SAED patterns of LPSO.

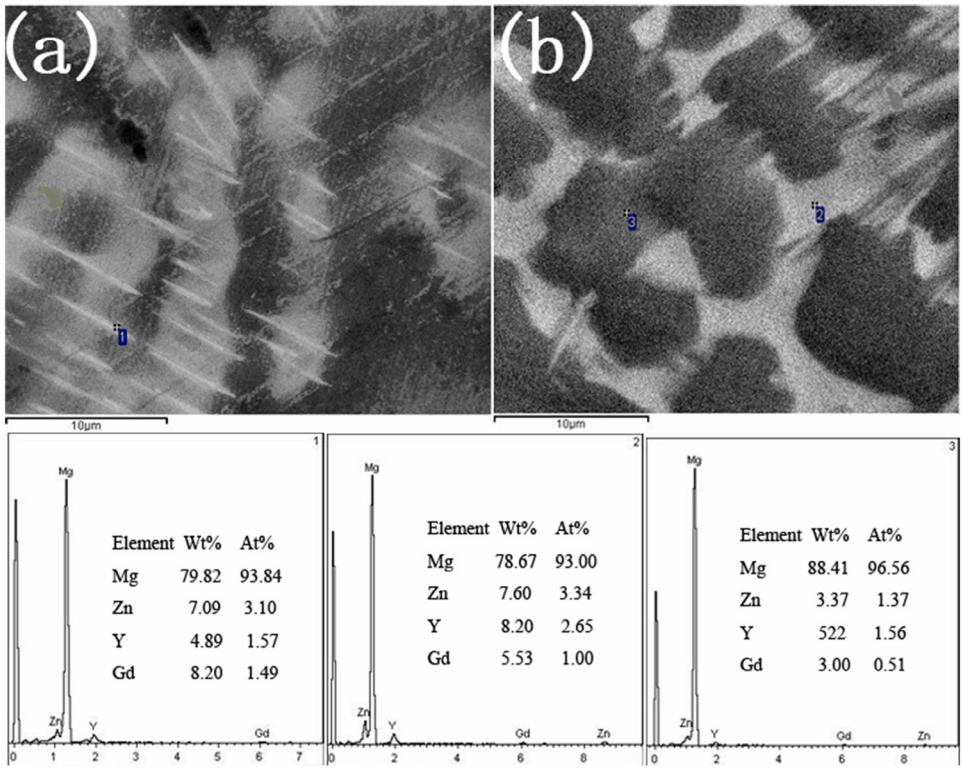

Fig. 4. SEM and EDS of $Mg_{97-x}Zn_1Y_2Gd_x$ alloys: (a) $Mg_{97}Y_2Zn_1$; (b) $Mg_{96.5}Y_2Zn_1Gd_{0.5}$.

according to polarization curves, hydrogen evolution and mass loss with the computational equation of corrosion rates provided by the reference [21].

Fig. 6 shows the polarization curves of the $Mg_{97-x}Y_2Zn_1Gd_x$ alloys. It can be seen that the corrosion potential decreases to −.551V from −0.885V with the increase of Gd addition. One reason is that the increase of Gd component of the α-Mg and eutectic phase decreases the potential difference (Fig. 4). The corrosion rates were calculated and presented in Table 2. It can be seen that the i_{corr} has a lowest value that is 2.1×10^{-3} mA.cm^{-2} for MG0.5 alloy. The corrosion rates curves of mass loss and hydrogen evolution were presented in Fig. 7. In general, the negative difference effect occurs in the all experimental alloy. The corrosion rates increases gradually with the increasing time in the hydrogen evolution and mass loss investigation. But the slope of increasing becomes slow.

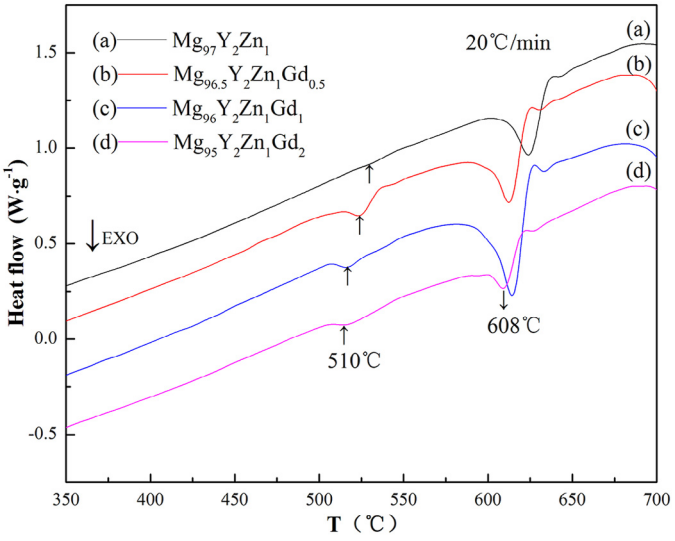

Fig. 5. The DSC patterns of $Mg_{97-x}Y_2ZnGd_x$ alloys: (a) $Mg_{97}Y_2Zn_1$; (b) $Mg_{96.5}Y_2Zn_1Gd_{0.5}$; (c) $Mg_{96}Y_2Zn_1Gd_1$; (d) $Mg_{95}Y_2Zn_1Gd_2$.

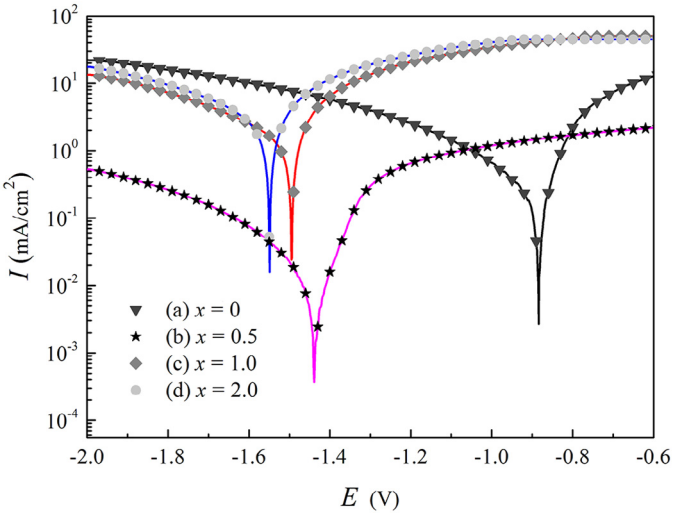

Fig. 6. The polarization curves of the $Mg_{97-x}Y_2ZnGd_x$: (a) $Mg_{97}Y_2Zn_1$; (b) $Mg_{96.5}Y_2Zn_1Gd_{0.5}$; (c) $Mg_{96}Y_2Zn_1Gd_1$; (d) $Mg_{95}Y_2Zn_1Gd_2$.

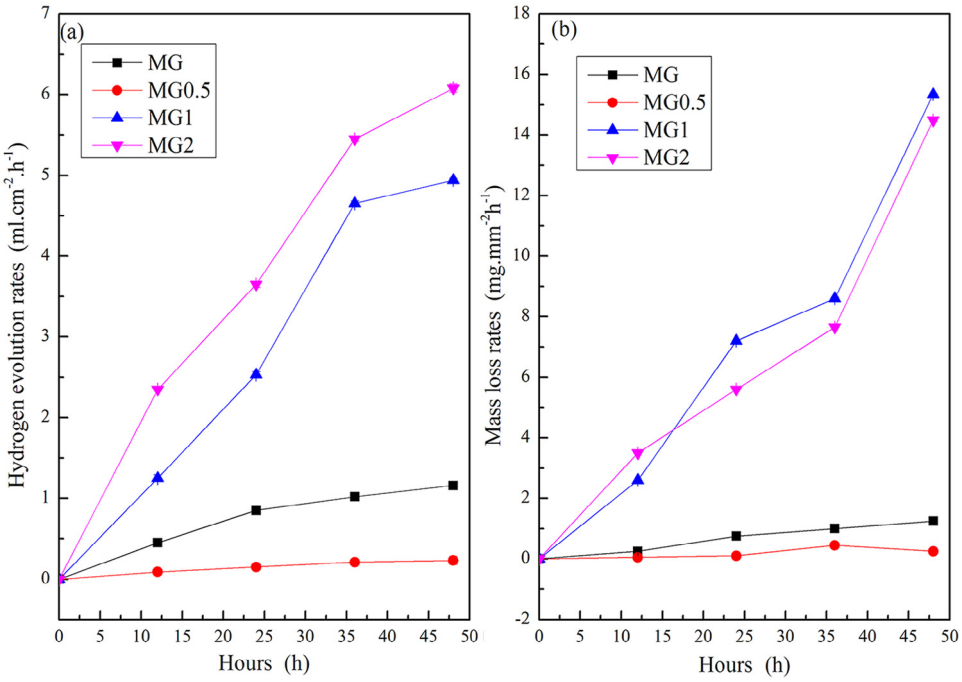

Fig. 7. The corrosion rates of hydrogen evolution rate and mass loss rates: (a) hydrogen evolution rate; (b) mass loss rates.

In the mass loss testing, the corrosion rate of MG1 alloy is slightly higher than that of MG2 alloy after 17 hours. The phenomenon is composed of the polarization test results. It can be illustrated that there are different corrosion mechanisms in the MG1 alloy and MG2 alloy. It will be further discussed in next part. The corrosion rate of MG0.5 alloy has the minimum value of 0.05 ± 0.001 (mm.year^{-1}) corresponding to polarization curve, 11.55 ± 1.5 (mm.year^{-1}) corresponding to mass loss and 11.44 ± 1.23 (mm.year^{-1}) corresponding to hydrogen evolution in Tables 2 and 3.

Corrosion morphologies of $Mg_{97-x}Y_2Zn_1Gd_x$ (as $x = 0$, 0.5, 1, 2at. %) alloys are shown in Fig. 8. The investigated alloys exhibit different corrosion type. The general corrosion occurs on the surfaces of MG, MG0.5 and MG2 alloys, while the local corrosion presents on the surfaces of MG1 alloys. Fig. 9 presents the corrosion morphology of alloys after removing the corrosion products. It can be seen that the LPSO phase can be found in the general corrosion. But the α-Mg has much damage. Meanwhile, there are many corrosion pits in the MG1 alloy. It can be seen that the eutectic phase joins in the corrosion reaction as the cathode in alloys. The α-Mg lost electrons are regarded as the anode. On the earlier stage of the reaction, the dissolution of α-Mg is along the boundary. The anodic reaction consisted of alloy dissolution as follows [22,24].

Table 2
The results of dynamic potential polarization curve.

Alloy	I_{corr} (mA/cm^2)	E_{corr} (V)	ν(mm.year^{-1})
MG	86.5 ± 2.35	−0.885±0.004	2.07 ± 0.051
MG0.5	2.1 ± 2.05	−1.439±0.005	0.05 ± 0.001
MG1	260.5 ± 2.03	−1.498±0.004	6.81 ± 0.052
MG2	225.7 ± 1.98	−1.551±0.005	5.43 ± 0.021

Table 3
The corrosion rate of mass loss rates and hydrogen evolution rate (48h).

Alloy	Mass loss		Hydrogen evolution	
	(mg.cm^{-2} h^{-1})	(mm.year^{-1})	(ml.cm^{-2} h^{-1})	(mm.year^{-1})
MG	1.25 ± 0.05	59.11 ± 1	1.16 ± 0.02	57.55 ± 1.2
MG0.5	0.25 ± 0.01	11.55 ± 1.5	0.23 ± 0.05	11.44 ± 1.23
MG1	15.34 ± 0.02	693.11 ± 2.35	4.94 ± 0.02	246.13 ± 3.25
MG2	17.49 ± 0.05	756.78 ± 3.5	6.08 ± 0.05	304.21 ± 3.12

Anodic reaction: $Mg \rightarrow Mg^{2+} + 2e^-$ (1)

In aerated 3%NaCl solution, electrons were produced by above anodic reaction and were consumed by the reaction of water that was transformed into OH^- by cathodic reaction. The following cathodic reaction may occur [25,26].

Cathodic reaction: $2H_2O + 2e^- \rightarrow H_2\uparrow + 2OH^-$ (2)

4. Discussions

The microstructures of alloys play an important role in corrosion resistance [27]. The Gd addition has a noticeable influence on the microstructure of Mg–Zn–Y alloy. The surface of MG alloy has small volume fraction LPSO phase, and the MG0.5 alloy has the complete network, uniformity and large volume fraction of LPSO phase. The MG1 alloy has some eutectic phase and a small amount of LPSO phase, while the MG2 alloy corresponds to the large volume fraction of eutectic phase. Besides, the Gd addition has a significant effect on corrosion types. As is well known, the corrosion types mainly include general corrosion and local corrosion. The general corrosion morphologies occur in MG, MG0.5 and MG2 alloys,

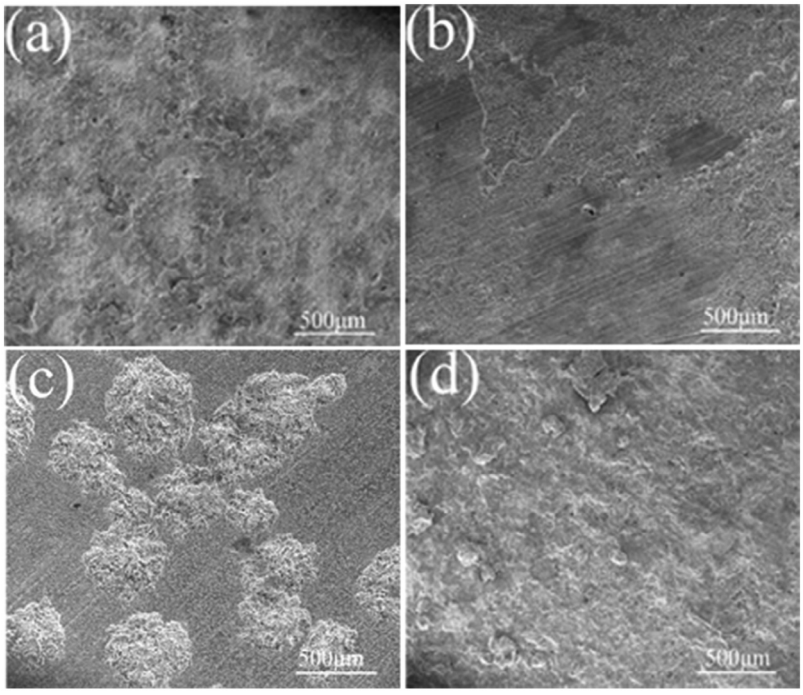

Fig. 8. The corrosion surfaces after removing corrosion production: (a) $Mg_{97}Y_2Zn_1$; (b) $Mg_{96.5}Y_2Zn_1Gd_{0.5}$; (c) $Mg_{96}Y_2Zn_1Gd_1$; (d) $Mg_{95}Y_2Zn_1Gd_2$.

while the local corrosion occurs in the MG1 alloy. Generally, the local corrosion includes two types [28]. The first type consists in most alloys with passivation layer after the breakdown of passive film. The second type occurs in some alloy without passivation. Although corrosion occurs on the entire surface of materials, the distribution of corrosion rate is very uneven, i.e., the corrosion rate of one part is significantly greater than that of another part. Obviously, the corrosion type of MG1 alloy belongs to the second type. It is supported by corrosion pits on the surface of MG1 alloy. The reason may be the nonhomogeneous distribution of LPSO phase and component composition in MG1 alloy. In addition, though the corrosion potential decreases with the increase of Gd addition in investigated alloy, the corrosion rates of MG0.5 alloy is smaller than other alloys.

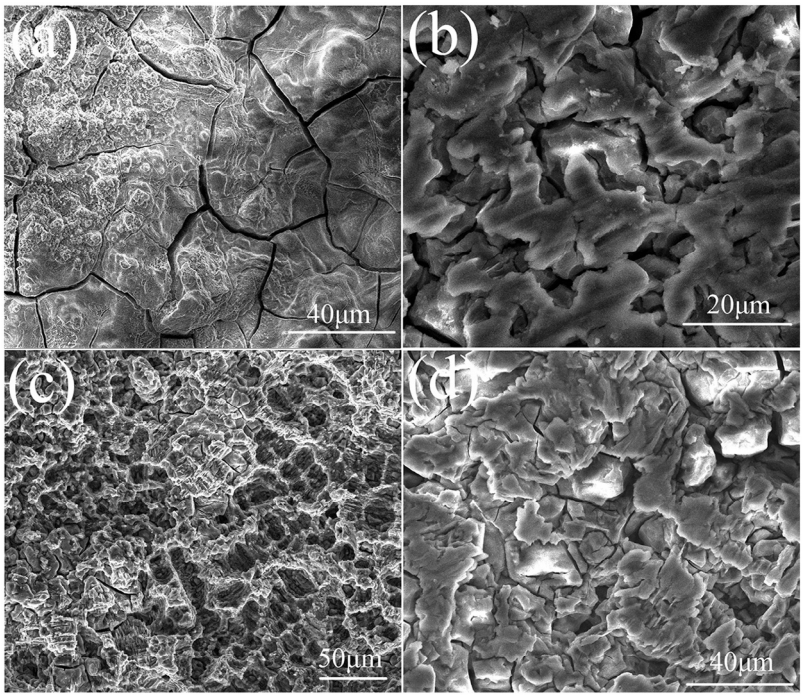

Fig. 9. The local observation corrosion surfaces after removing corrosion production: (a) $Mg_{97}Y_2Zn_1$; (b) $Mg_{96.5}Y_2Zn_1Gd_{0.5}$; (c) $Mg_{96}Y_2Zn_1Gd_1$; (d) $Mg_{95}Y_2Zn_1Gd_2$.

The reason may be that the uniformity network-LPSO phase results in the lower self-corrosion current density than other alloys. Therefore, it can be seen that the Gd addition has a noticeable effect on the microstructure of the Mg–Zn–Y alloys, and the distribution, volume fraction and Gd content of LPSO phase further dominate corrosion types and corrosion resistance.

5. Conclusions

1 When the atomic fraction of Zn is 1% and the atomic ratio of Zn/RE (Y, Gd) is 2:5, the volume fraction of LPSO phase can reach the extreme value. Moreover, the average grain size has become much smaller with Gd addition.

2 The corrosion potential shows a decreasing trend with Gd addition. The $Mg_{97-x}Zn_1Y_2Gd_x$ alloys has better corrosion resistance as $x = 0.5$. For the MG0.5 alloy, the complete network microstructures and large volume fraction of LPSO phase lead to the better corrosion resistance.

Acknowledgments

This work is supported by the Special Joint Funds of Natural Science Foundation of Shandong Province, China (ZR2013EML004) and the National Natural Science Foundation of China (51571102, 51401085).

References

[1] Y.G. Li, Y.H. Wei, L.F. Hou, P.J. Han, Corros. Sci. 69 (2013) 67–76.
[2] X.B. Zhang, Y.J. Yuan, L. Mao, J.L. Niu, W.J. Ding, Mater. Lett. 86 (2012) 42–45.
[3] H. Somekawa, H. Watanabe, T. Mukai, Mater. Lett. 65 (2011) 3251–3253.
[4] M. Rashad, F. Pan, W. Guo, H. Lin, M. Asif, M. Irfan, Mater. Charact. 106 (2015) 382–389.
[5] X. Zhao, L.L. Shi, J. Xu, J. Mater. Sci. Technol. 29 (2013) 781–787.
[6] A.A. Luo, J. Mag. Alloys 1 (2013) 2–22.
[7] Y. Tian, H. Huang, G.Y. Yuan, C.L. Chen, Z.C. Wang, W.J. Ding, Mater. Lett. 130 (2014) 236–239.
[8] D. Wang, J.S. Zhang, J.D. Xu, J.D. Xu, Z.L. Zhao, W.L. Cheng, et al., J Mag. Alloys 2 (2014) 78–84.
[9] P. Chen, D.L. Li, J.X. Yi, B.Y. Tang, L.M. Peng, W.J. Ding, J. Alloys Compd. 485 (2009) 672–676.
[10] X. Li, C. Liu, Mater. Lett. 65 (2011) 1726–1729.
[11] C. Xu, M.Y. Zheng, Y.Q. Chi, X.J. Chen, K. Wu, E.D. Wang, et al., Mater. Sci. Eng: A 549 (2012) 128–135.
[12] H.P. Zhou, L.X. Hu, H.F. Sun, X.J. Chen, Mater. Charact. 106 (2015) 44–51.
[13] F.M. Lu, A.B. Ma, J.H. Jiang, D.H. Yang, Q. Zhou, Rare Met. 31 (2012) 303–310.
[14] Z.W. Zhao, X.Y. Teng, G.R. Zhou, J.F. Leng, J.W. Geng, Rare Met. 43 (2014) 791–795.
[15] J.W. Geng, X.Y. Teng, G.R. Zhou, D.G. Zhao, Mater. Lett. 132 (2014) 334–337.
[16] M. Li, K. Zhang, Z.W. Du, X.G. Li, Y.J. Li, M.L. Ma, et al., Mater. Charact. 109 (2015) 66–72.
[17] Y. Kawamura, K. Hayashi, A. Inoue, T. Masumoto, Mater. Trans. 51 (2004) 107–111.
[18] G. Song, A. Atrens, Adv. Eng. Mater. 5 (2003) 837–858.
[19] Y. Kawamura, M. Yamasaki, Mater. Trans. 11 (2007) 2986–2992.
[20] Y.L. Ju, D.H. Kim, H.K. Lim, D.H. Kim, Mater. Lett. 59 (2005) 3801–3805.
[21] Z.M. Shi, M. Liu, A. Atrens, Corros. Sci. 52 (2010) 579–588.
[22] G.L. Song, A. Atrens, Adv. Eng. Mater. 1 (1999) 11–33.
[23] A. Atrens, G. Song, M. Liu, Z. Shi, F. Cao, M.S. Dargusch, Adv. Eng. Mater. 17 (2015) 400–453.
[24] W.A. Ferrando, J. Mater. Eng. 11 (1989) 299–313.
[25] G. Song, A. Atrens, D. Stjohn, J. Nairn, Y. Li, Corros. Sci. 39 (1997) 855–875.
[26] G. Song, A. Atrens, M. Dargusch, Corros. Sci. 41 (1999) 249–273.
[27] M.J. Moradi, M. Ketabchi, Materialprufung 58 (2016) 48–55.
[28] E. Ghali, W. Dietzel, K.U. Kainer, E. Ghali, W. Dietzel, K.U. Kainer, J. Mater. Eng. Perform. 13 (2004) 7–23.